International Journal of Solids and Structures 49 (2012) 3488–3495

Contents lists available at SciVerse ScienceDirect

International Journal of Solids and Structures

journal homepage: www.elsevier.com/locate/ijsolstr

Material modeling of 6000 series aluminum alloy sheets with different density cube textures and effect on the accuracy of finite element simulation

Daisaku Yanaga [a], Toshihiko Kuwabara [b,*], Naoyuki Uema [c], Mineo Asano [c]

[a] Department of Mechanical Systems Engineering, Graduate School of Engineering, Tokyo University of Agriculture and Technology, 2-24-16, Nakacho, Koganei-shi, Tokyo 184-8588, Japan
[b] Division of Advanced Mechanical Systems Engineering, Institute of Engineering, Tokyo University of Agriculture and Technology, 2-24-16, Nakacho, Koganei-shi, Tokyo 184-8588, Japan
[c] Research & Development Center, Sumitomo Light Metal Industries, Ltd., 3-1-12 Chitose, Minato-ku, Nagoya 455-8670, Japan

ARTICLE INFO

Article history:
Available online 21 March 2012

Keywords:
Aluminum alloy
Anisotropy
Biaxial tension
Cruciform specimen
Experimental techniques
Finite element analysis
Hydraulic bulge test
Texture
Yield function

ABSTRACT

Biaxial tensile tests of 6000 series aluminum alloy sheet with different density cube textures were conducted using cruciform specimens. The specimens were loaded under linear stress paths in a servo-controlled biaxial tensile testing machine. The plastic orthotropy remained coaxial with the principal stresses throughout every experiment. Successive contours of plastic work in stress space and the directions of plastic strain rates were precisely measured and compared with those calculated using selected yield functions. The Yld2000-2d yield functions with exponents of 12 and 6 were capable of reproducing the general work contour trends and the directions of plastic strain rates observed for the test materials with high and low density cube textures, respectively. Hydraulic bulge tests were also conducted and the variation of thickness strain along the meridian directions of the bulged specimen was compared with that calculated using finite element analysis (FEA) based on selected yield functions. Differences in the cube texture density caused significant differences in the strain distribution of the bulged specimens, and were in good agreement with the FEA results obtained using the Yld2000-2d yield functions. It is thus concluded that the biaxial tensile testing method with a cruciform specimen is an effective material testing method for accurately detecting and modeling the deformation behavior of sheet metals under biaxial tension.

1. Introduction

Lightening the weight of automotive bodies is effective in reducing CO_2 emissions. It is an important step towards the preservation of the Earth's environment. Since aluminum alloy sheet is lighter than steel sheet, it is regarded as a material candidate for reducing the weight of automobiles. However, aluminum alloy sheets are generally inferior in ductility to steel sheets and are therefore difficult to use for the manufacture of automotive body panels.

There are two countermeasures to enhance the use of aluminum alloy sheet for automotive body panels. One is to build an appropriate texture into the aluminum alloy sheet to provide good formability. For example, Yoshida et al. (2007) investigated the effect of aluminum alloy sheet texture on the forming limit strains using a Marciniak–Kuczyński-type approach and a generalized Taylor-type polycrystal model, and demonstrated that only a cube texture component yields forming limits much higher than random texture in the biaxial stretch range. The other countermeasure is to improve the predictive accuracy of forming simulations, such as finite element analysis (FEA), to minimize the time and cost required in designing the tool geometry and forming conditions for the manufacture of aluminum alloy body panels. In order to improve the predictive accuracy of forming simulations, it is necessary to use a material model that is capable of accurately reproducing the deformation behavior of the material (Kuwabara, 2007; Banabic et al., 2010).

The crystallographic textures of rolled sheet metals have a significant effect on the deformation characteristics and formability of the material (Barlat, 1987; Kuwabara et al., 2002; Yoshida et al., 2007). In sheet metal forming simulations, the difference in the deformation characteristics of real sheet metals caused by the crystallographic texture is expected to be reproduced by the yield functions employed. Therefore, validation of this notion is crucial to deepen our knowledge of the effects and limitations of yield functions on the accuracy of forming simulations based on the phenomenological theory of plasticity. Yoon et al. (2006) performed cup drawing simulations of an aluminum alloy sheet to predict the cup height profile and concluded that an accurate prediction of the earing profile can be obtained only if the anisotropy of the tensile properties (flow stresses and *r*-values) are captured very accurately using the Yld2004-18p yield function proposed by Barlat et al. (2005). Kuwabara et al. (1998) developed a biaxial

* Corresponding author. Tel.: +81 42 388 7083; fax: +81 42 385 7204.
E-mail address: kuwabara@cc.tuat.ac.jp (T. Kuwabara).

0020-7683/$ - see front matter © 2012 Elsevier Ltd. All rights reserved.
http://dx.doi.org/10.1016/j.ijsolstr.2012.03.005

Table 1
Mechanical properties of the test materials.

Texture	Tensile direction [°]	$\sigma_{0.2}$ [MPa]	c* [MPa]	n^*	α^*	r-value**
High	0	169	494	0.24	0.008	0.54
Cube	45	152	469	0.28	0.014	0.13
(HC)	90	163	485	0.25	0.007	0.55
Low	0	152	474	0.25	0.007	0.80
Cube	45	146	469	0.27	0.009	0.26
(LC)	90	145	466	0.26	0.007	0.70

* Parameters for Swift's hardening law, $\sigma = c(\alpha + \varepsilon^p)^n$, for the strain range of $0.002 \leqslant \varepsilon^p \leqslant \varepsilon^p_B$, where ε^p_B is the true plastic strain at the maximum load.
** Measured at a uniaxial nominal strain of 0.10.

tensile testing method for sheet metals using a cruciform specimen, and demonstrated that it is necessary to select appropriate yield functions for sheet metals used in the measurement to improve the predictive accuracy of FEA simulations for hole expansion (Hashimoto et al., 2010; Kuwabara et al., 2011) and shallow shell drawing of automotive body panels (Moriya et al., 2010).

This study aims to clarify the accuracy of yield functions in order to reproduce differences in plastic deformation behavior caused by differences in crystallographic textures. Two types of 6016 aluminum alloy sheet are used, which have the same chemical composition but different cube texture densities. An appropriate yield function for each test material was first determined by biaxial tensile tests with linear stress paths using cruciform specimens. Hydraulic bulge tests were then conducted to apply large biaxial plastic deformation to the test materials. The thickness strain distribution along the meridian directions of the bulged specimen was measured to investigate the effect of crystallographic texture differences on the deformation behavior of the aluminum alloys. Finally, FEA simulations of the hydraulic bulging tests were conducted using an appropriate yield function determined from the biaxial tensile tests. The calculated thickness strains were compared to the measured thickness strains to reveal the effect of the yield functions on the accuracy of the FEA for the hydraulic bulge test.

2. Test material

Two types of 6016-T4 aluminum alloy sheet (Al-1.0Si-0.5Mg-0.1Mn (mass%), 0.9 mm thick) were prepared with different cube orientation intensities at the 1/4 thickness position of 133 and 21 (at random), which are referred to as High Cube (HC) and Low Cube (LC), respectively. The work hardening characteristics and r-values in different directions from the rolling direction are listed in Table 1. In order to reduce the effect of natural age hardening on the experimental results as much as possible, the material was aged at room temperature for two years prior to the experiments.

Fig. 1 shows uniaxial true stress-true plastic strain curves of the test materials for different directions from the rolling direction.

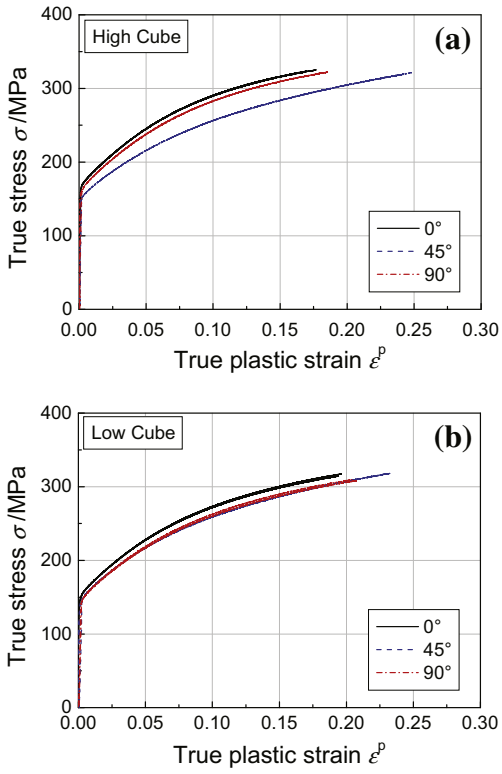

Fig. 1. Uniaxial true stress-true plastic strain curves for the test materials. The end point of each curve corresponds to the maximum load point.

3. Biaxial tensile test procedures and results

3.1. Experimental method

Biaxial tensile tests were performed using the cruciform specimen shown in Fig. 2 to determine the appropriate anisotropic yield functions that are capable of reproducing the elastic-plastic deformation behavior of the test materials. The geometry of the specimen is similar to that used by Kuwabara et al. (1998, 2000, 2002). Each arm of the specimen has seven slits, 30 mm long and 0.2 mm wide, at 3.75 mm intervals to reduce the geometric constraint on the deformation of the 30×30 mm^2 square gauge section as much as possible. The specimens were cut from as-received large flat rolled sheet samples using laser machining so that the arms were parallel

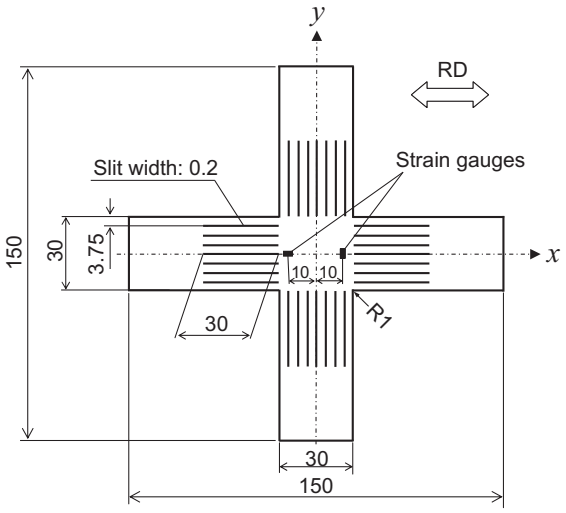

Fig. 2. Cruciform specimen used for the biaxial tensile test (dimensions in mm).

to the rolling (RD) and transverse (TD) directions of the sheet. The slits were also fabricated by laser machining. The RD, TD and thickness direction of a specimen are defined as the *x*-, *y*- and *z*-axes, respectively.

Biaxial tensile forces (F_x,F_y) were applied to the cruciform specimen using a servo-controlled biaxial tensile testing machine developed by Kuwabara et al. (1998). The nominal tensile stress components (σ_{Nx}, σ_{Ny}) were in fixed proportions during each test; σ_{Nx}:σ_{Ny} = 1:0, 4:1, 2:1, 4:3, 1:1, 3:4, 1:2, 1:4 and 0:1. The biaxial total strain components (ε_x,ε_y) were measured using two uniaxial strain gauges (Tokyo Sokki Kenkyujo, YFLA-2) mounted on the centerlines of the specimens at (x,y) = (±10 mm, 0) for the tests of σ_{Nx}:σ_{Ny} = 4:1, 2:1, 4:3 and 1:1, and at (x,y) = (0,±10 mm) for the tests of σ_{Nx}:σ_{Ny} = 3:4, 1:2 and 1:4. The true stress components (σ_x, σ_y) were determined by dividing (F_x,F_y) by the current cross-sectional area of the gauge section, which was determined from measurements of the true plastic strain components (ε_x^p, ε_y^p) with an assumption of constant volume. σ_{xy} was assumed to be zero, because ε_x and ε_y were measured on the centerlines of the specimen. For σ_{Nx}:σ_{Ny} = 1:0 and 0:1, standard uniaxial tensile specimens (JIS 13 B-type) were used. The equivalent plastic strain rate was 1 to 4 × 10^{-4} s^{-1}.

According to the FEA of the cruciform specimen and the strain measurement position shown in Fig. 2, the error of the stress measurement was estimated to be less than 2% using selected isotropic (von Mises) and anisotropic yield functions for the material models (Hanabusa et al., 2010, 2011).

In this study, the concept of the contour of plastic work in the stress space (Hill and Hutchinson, 1992; Hill et al., 1994) was used to evaluate the work hardening behavior of the test materials under biaxial tension. The stress–strain curve obtained from a uniaxial tensile test along the RD of the material was selected as a reference datum for work hardening; the uniaxial true stress σ_0 and the plastic work per unit volume W_0 corresponding to particular values of offset logarithmic plastic strains ε_0^p were determined. The uniaxial true stress σ_{90} obtained from a uniaxial tensile test along the TD and the biaxial true stress components (σ_x,σ_y) obtained from biaxial tensile tests were then determined at the same plastic work as W_0. The stress points (σ_0,0), (0,σ_{90}) and (σ_x,σ_y) plotted in the principal stress space comprise a contour of plastic work corresponding to a particular value of ε_0^p. For a sufficiently small value of ε_0^p the corresponding work contour can be practically viewed as a yield locus.

3.2. Experimental results

Fig. 3 shows the measured stress points that comprise the contours of plastic work. All stress values comprising a work contour are normalized by σ_0 corresponding to a specific value of ε_0^p. The maximum values of ε_0^p for which (σ_x,σ_y) could be measured for all stress paths were 0.040 for HC and 0.045 for LC. Both HC and LC exhibit differential work hardening; the normalized work contours show a tendency to contract with an increase of ε_0^p, except that the stress points for σ_{Nx}:σ_{Ny} = 1:1 and 0:1 remain almost on a single point. The shape of the work contours of HC is close to the Tresca type with a sharp corner in the vicinity of equibiaxial tension, while that of LC bulges more in the vicinity of the plane strain tension region (σ_{Nx}:σ_{Ny} = 2:1 and 1:2) than HC. Table 2 shows the measured stress values comprising the work contours for ε_0^p = 0.040 (HC) and 0.045 (LC).

The theoretical yield loci based on the von Mises (Von Mises, 1913), Hill's quadratic (Hill, 1948), and the Yld2000-2d yield functions (Barlat et al., 2003; Yoon et al., 2004) are superimposed in the figure. The unknown parameters of the Hill's quadratic yield function were determined using r_0, r_{45}, r_{90} and σ_0/σ_0, and those of the Yld2000-2d yield function were determined using r_0, r_{45}, r_{90} and r_b

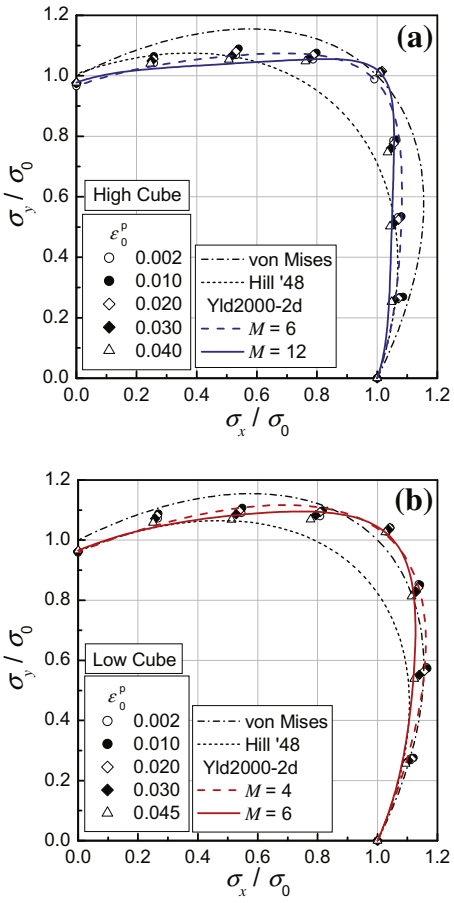

Fig. 3. Measured stress points comprising contours of plastic work compared with the theoretical yield loci. Each symbol corresponds to a contour of plastic work for a particular value of ε_0^p. The exponents *M*, selected for the Yld2000-2d yield function were 6 for HC and 4 for LC with $\varepsilon_0^p = 0.002$, 12 for HC with $\varepsilon_0^p = 0.040$, and 6 for LC with $\varepsilon_0^p = 0.045$.

and σ_0/σ_0, σ_{45}/σ_0, σ_{90}/σ_0 and σ_b/σ_0, where r_α and σ_α are the *r*-value and tensile flow stress measured at an angle α from the RD, respectively, and where r_b and σ_b are the ratio of the plastic strain increments, $d\varepsilon_y^p/d\varepsilon_x^p$, and the flow stress at equibiaxial tension, σ_{Nx}:σ_{Ny} = 1:1, respectively. The values of r_0, r_{45} and r_{90} used were the same as those in Table 1, both for the Hill '48 and Yld2000-2d yield functions. The values of σ_{45}/σ_0, σ_{90}/σ_0, σ_b/σ_0 and r_b used to determine the Yld2000-2d yield function correspond to those comprising the work contours shown in the figure. The exponent *M* of the Yld2000-2d yield function was determined, as will be explained later in the paper, to give the smallest standard deviation

Table 2
Measured stress values comprising work contours.

Texture	High cube		Low cube	
ε_B^p	0.040		0.045	
σ_0 [MPa]	233.76		223.26	
σ_{Nx}/σ_{Ny}	σ_x/σ_0	σ_y/σ_0	σ_x/σ_0	σ_y/σ_0
1:0	1.0000	0.0000	1.0000	0.0000
4:1	1.0477	0.2520	1.0936	0.2560
2:1	1.0430	0.5020	1.1229	0.5384
4:3	1.0350	0.7470	1.1142	0.8126
1:1	1.0096	1.0103	1.0264	1.0257
3:4	0.7618	1.0477	0.7765	1.0684
1:2	0.5074	1.0532	0.5123	1.0682
1:4	0.2456	1.0393	0.2508	1.0579
0:1	0.0000	0.9775	0.0000	0.9654

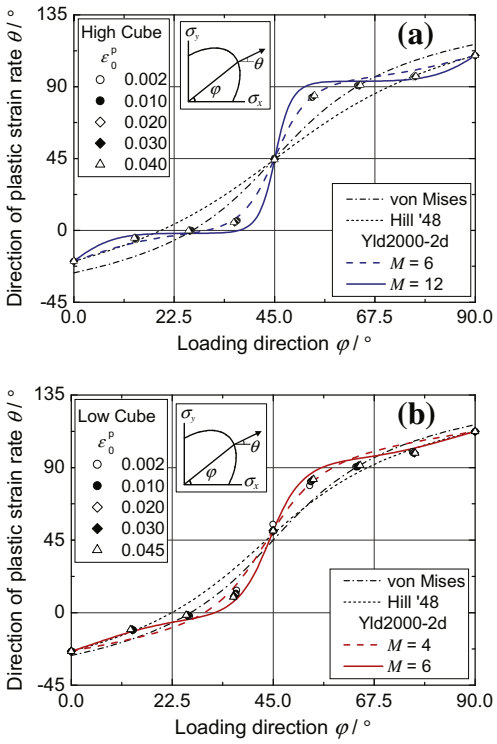

Fig. 4. Comparison of the directions of measured plastic strain rates with those of the local outward vectors normal to the yield loci calculated using selected yield functions.

of the calculated yield locus from the corresponding work contour. Consequently, for HC, M was determined to be 6 for $\varepsilon_0^p = 0.002$, and 12 for $\varepsilon_0^p = 0.04$. For LC, M was determined to be 4 for $\varepsilon_0^p = 0.002$, and 6 for $\varepsilon_0^p = 0.045$. Thus, the Yld2000-2d yield function has the best agreement with the work contours for both materials.

In order to validate the normality flow rule for the selected yield functions, the directions θ of the plastic strain rates were measured for all linear stress paths and compared with those calculated using the yield functions (the directions of outward vectors normal to the theoretical yield locus). The results are shown in Fig. 4, where φ is the loading angle of a stress path from the x-axis in the principal stress space, and both θ and φ are defined to be zero along the x-axis and positive in the anti-clockwise direction. The Yld2000-2d yield function again provides the closest agreement with the measurement.

To obtain a more quantitative evaluation of the reproducibility of the work contours and the directions of plastic strain rates using the selected yield functions, the standard deviations, S_r and S_θ, were calculated using the following equations:

$$S_r = \sqrt{\frac{\sum_{i=1}^{9}(r_i' - r_i)^2}{8}} \tag{1a}$$

$$S_\theta = \sqrt{\frac{\sum_{i=1}^{9}(\theta_i' - \theta_i)^2}{8}} \tag{1b}$$

where φ_i (i: 1–9) is the loading angle of the ith stress point from the x-axis in the principal stress space (see schematic in Fig. 5), r_i is the distance between the origin in the principal stress space and the ith stress point, r_i' is the distance between the origin in the principal stress space and the intersection of the theoretical yield locus, and the stress path in the direction φ_i, and θ_i and θ_i' are the measured and calculated directions of the plastic strain rates at the stress point i, respectively.

Fig. 5 shows the variation of S_r and S_θ with increasing ε_0^p. For HC, the prediction using the Yld2000-2d yield function with $M = 6$ has the closest agreement with the work contours and the directions of plastic strain rates at the early stage of plastic deformation ($\varepsilon_0^p \le 0.01$). On the other hand, as ε_0^p increases, the shape of the work contours changes gradually to approach the Yld2000-2d yield function with $M = 12$–14, while the variation of the directions of plastic strain rates are small. For LC, the prediction using the Yld2000-2d yield function with $M = 4$ has the closest agreement with the work contours and the directions of plastic strain rates for $\varepsilon_0^p \le 0.01$, while the optimum value of M that is capable of reproducing the work contours, and the direction of plastic strain rates approaches 6 with increasing ε_0^p.

The von Mises and Hill '48 yield functions are inferior to the Yld2000-2d yield function with respect to reproducibility of the test material deformation behavior.

4. Hydraulic bulge test procedures and results

4.1. Experimental method

Hydraulic bulge tests were performed and the thickness distribution along the meridian directions of the bulged specimens was measured to quantitatively evaluate the effect of the difference in crystallographic texture on the deformation behavior of the test materials.

Fig. 6 shows the experimental apparatus used for the hydraulic bulge test. The diameter of the die opening was 150 mm, the die profile radius was 8 mm, and the blank diameter was 220 mm. The material flow-in was fixed at zero along the boundary of a 190 mm diameter using a triangular draw-bead. No lubricant was used at the interface between the blank and die surface.

The true total strain components, ε_x and ε_y, along the RD and TD of the original sheet were measured using a uniaxial strain gauge (Tokyo Sokki Kenkyujo Co., YFLA-2) attached at a distance of 5 mm in each direction from the center of the blank. The radius of curvature ρ at the top of the bulged specimen was measured 45° from the RD using a spherometer, as shown in Fig. 6. The gauge length was 40 mm. The spherometer can move in the vertical direction and rotate about the axis normal to the plane as shown in Fig. 6, so that it is always in contact with the bulged specimen at three points. The hydraulic pressure P was controlled so that the equivalent plastic strain rate was kept approximately constant (ca. 0.001 s^{-1}) during each test. The measured data of ε_x, ε_y, ρ and P were recorded every 0.1 s using a data logger.

The in-plane equibiaxial stress σ_b, at the top of the bulged specimen was measured as

$$\sigma_b = \frac{P\rho}{2t} \tag{2}$$

where t is the thickness at the top of the bulged specimen, determined using the equation

$$t = t_0\exp(\varepsilon_z) = t_0\exp(-\varepsilon_x - \varepsilon_y) \tag{3}$$

based on the condition of constant volume, in which the elastic strain components were neglected.

The strain gauges were replaced when $|\varepsilon_z| \approx 0.15$ and the bulge test was continued until $|\varepsilon_z| \approx 0.3$ to measure the $\sigma_b - |\varepsilon_z|$ curve. The equivalent stress $\bar{\sigma}$-equivalent plastic strain $\bar{\varepsilon}$ curve was determined using the equation

$$\bar{\sigma} = \sigma_b/\lambda \quad \text{and} \quad \bar{\varepsilon} = \lambda|\varepsilon_z^p|, \tag{4}$$

where λ is defined as the stress ratio σ_b/σ_0 measured at $\varepsilon_0^p = 0.04$ for HC and $\varepsilon_0^p = 0.045$ for LC.

A sheet specimen was bulged up to a height of 38 mm. It had an array of 10 mm^2 grids along the meridian directions 0, 45 and 90°

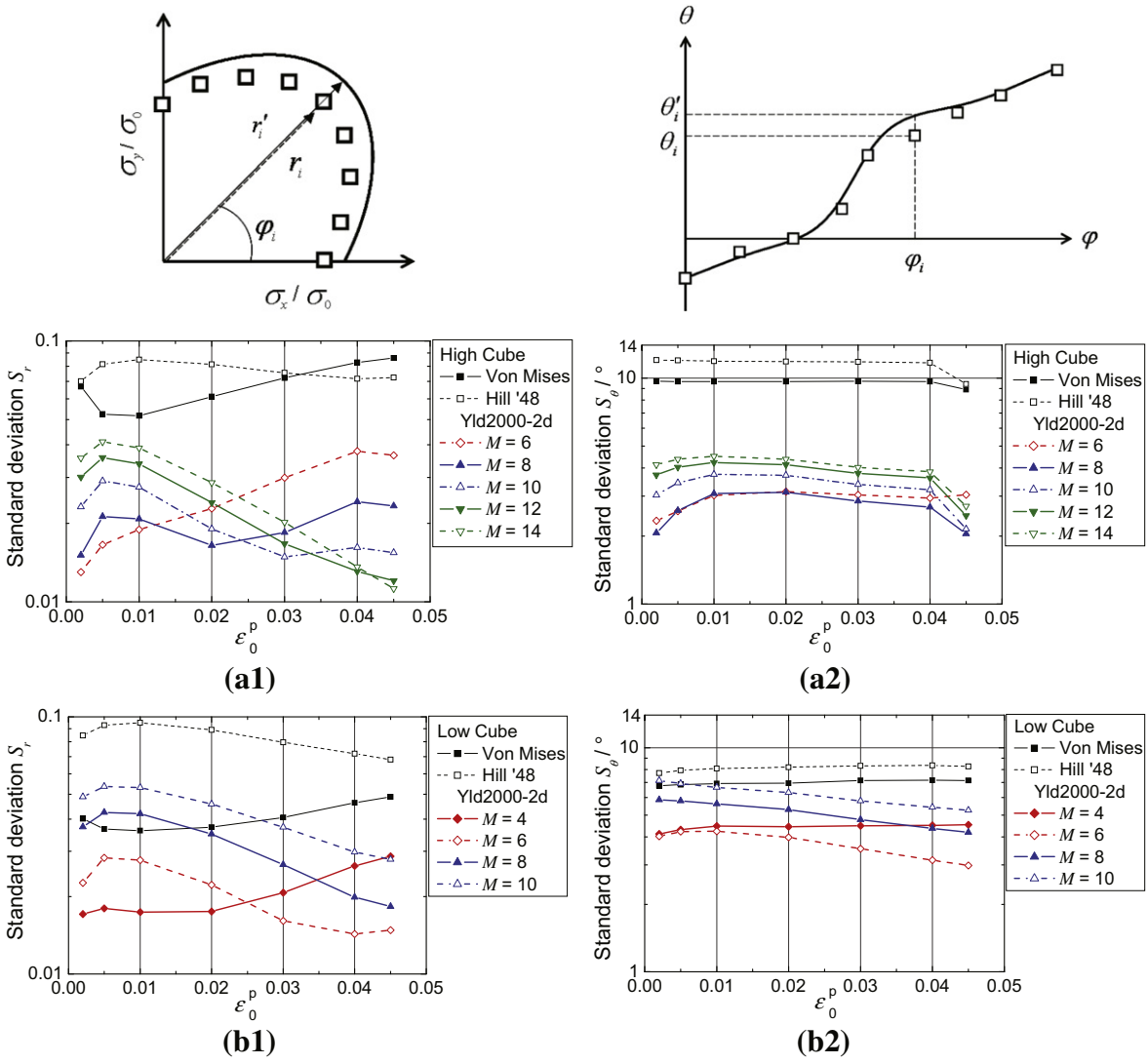

Fig. 5. Standard deviations for (a1) and (b1) work contours and (a2) and (b2) directions of plastic strain rates.

from the RD, for the measurement of the radial and circumferential plastic strains ($\varepsilon_r^p, \varepsilon_\theta^p$). After each bulge test, the thickness strain ε_z^p, was determined along the meridian lines as $\varepsilon_z^p = -\varepsilon_r^p - \varepsilon_\theta^p$.

4.2. 2 Experimental result

Fig. 7 shows the $\bar{\sigma} - \bar{\varepsilon}$ curve determined using Eq. (4) and the curve approximated using Swift's power law for the strain range of $\bar{\varepsilon} \leq 0.3$, the parameters of which are shown in Table 3. The work hardening curve determined from the uniaxial tensile test in the RD, which was approximated using Swift's power law (see Table 1), is also depicted in the figure for comparison. These work hardening curves were used in the FEA as described in Section 5.

5. Finite element analysis of hydraulic bulge forming

FEA simulations of the hydraulic bulge test were carried out using Abaqus/Standard Ver.6.9-1 (Abaqus Analysis, 2009). Fig. 8 shows the finite element mesh used for the analysis. One quarter of a circular blank was analyzed due to the orthotropic anisotropy of the material. The blank diameter was 190 mm and the nodal

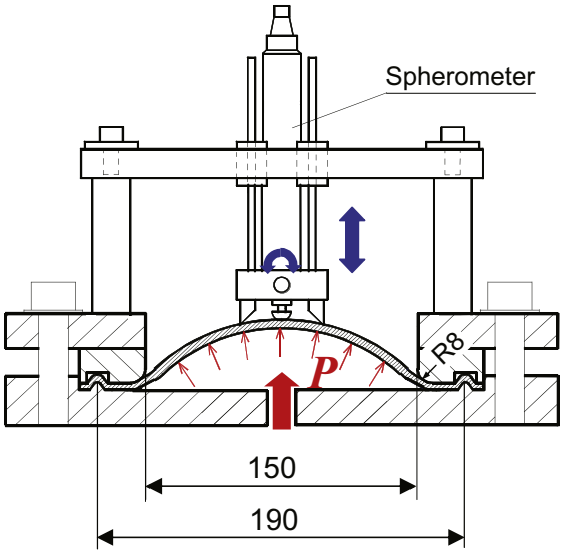

Fig. 6. Experimental apparatus for the hydraulic bulge test.

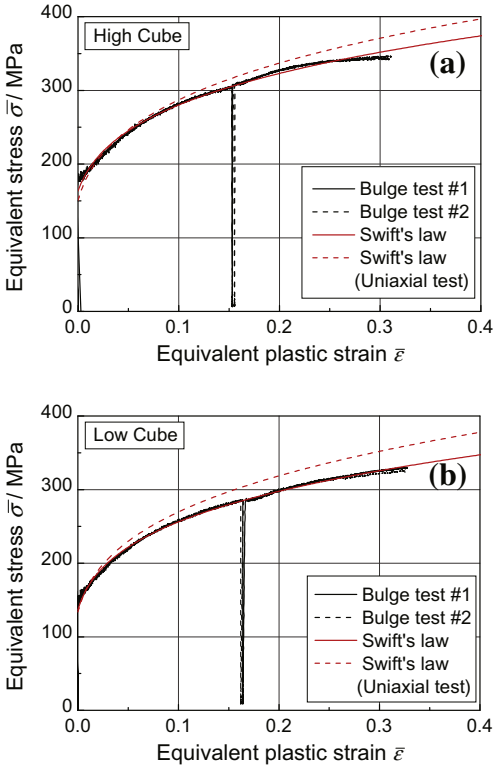

Fig. 7. Equivalent stress-equivalent plastic strain curves determined using the hydraulic bulge test data and those approximated using Swift's power law.

Table 3
Parameters for Swift's power law shown in Fig. 7.

Texture	λ^*	c^{**}[MPa]	n^{**}	α^{**}
HC	1.010	455	0.22	0.009
LC	1.026	426	0.23	0.007

* $\lambda \equiv \sigma_b/\sigma_0$, where σ_0 and σ_b are the uniaxial and equibiaxial stresses, respectively, comprising the work contour for $\varepsilon_0^p = 0.04$ (HC) and 0.045 (LC).
** Parameters for Swift's hardening law, $\sigma = c(\alpha + \varepsilon^p)^n$, determined for the strain range of $0.002 < \varepsilon^p < 0.30$.

displacement along the periphery of the blank was assumed to be zero, because the radial position of the draw-bead in the die used in the experiment was also 95 mm. 4-node shell elements, S4R, were used. The increment of element division was 2.5° in the circumferential direction and 1 mm in the radial direction for the range of radial coordinates 30 mm$\leqslant R \leqslant$ 95 mm. Mesh division was automatically performed in the range of $R \leqslant 30$ mm. A *surface-to-surface* contact condition of the blank to the die was selected with a blank holding force of 30 kN and a friction coefficient of 0.3. A bulge height of 38 mm was selected, the same as the experiment.

The yield functions used in the FEA were the von Mises (Von Mises, 1913), Hill's quadratic (Hill, 1948), and the Yld2000-2d yield functions (Barlat et al, 2003; Yoon et al., 2004), as shown in Fig. 3. The exponent of the Yld2000-2d yield function was chosen to be 12 for HC and 6 for LC, which gave the smallest S_r at $\varepsilon_0^p = 0.04$ and 0.045, respectively. Table 4 shows the anisotropic parameters of the Yld2000-2d yield function used in the FEA.

6. Results and discussion

Fig. 9 shows the measured thickness strain along the meridian lines, 0, 45 and 90° from the RD for the bulged specimens with a

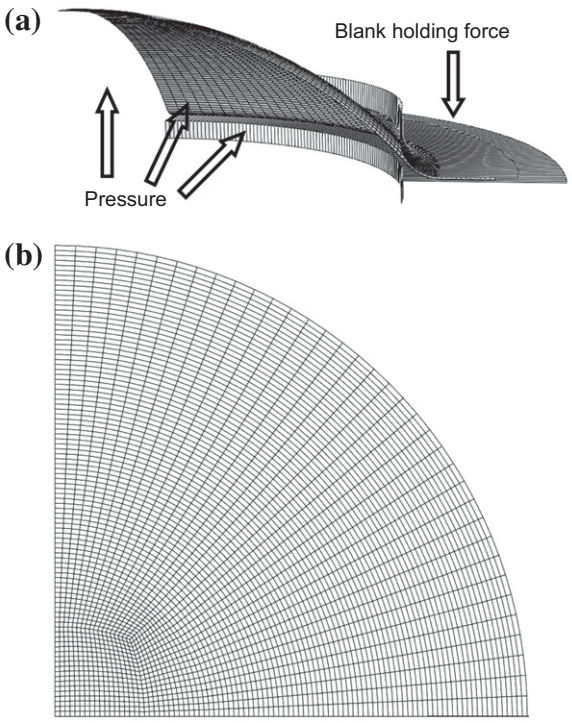

Fig. 8. Schematic illustration of the FEA model for the hydraulic bulge test; (a) tool, and (b) initial mesh division of a blank.

Table 4
Anisotropic parameters of the Yld2000-2d yield function used in the FEA.

Texture	High cube	Low cube
ε_0^p	0.040	0.045
Exponent	12	6
α_1	0.9418	0.9405
α_2	1.0082	1.0041
α_3	0.9243	0.8923
α_4	1.0181	1.0315
α_5	1.0095	0.9978
α_6	0.9610	0.8949
α_7	0.8045	0.7312
α_8	1.3614	1.3304

bulge height of 38 mm, compared with those calculated by FEA using selected yield functions. In Fig. 9(a), the equivalent stress-equivalent plastic strain curve used in the FEA was determined by approximating the measured uniaxial curve σ_x-ε_x^p, using Swift's power law (see Table 1), while in Fig. 9(b), the curve was determined by approximating the $\bar{\sigma} - \bar{\varepsilon}$ curve obtained from the hydraulic bulge test using Eq. (4) with Swift's power law (see Table 2).

Comparison of the experimental results between HC and LC clarified that $|\varepsilon_z^p|$ at the top of the bulged specimen is larger for LC than for HC, and $|\varepsilon_z^p|$ at the periphery (near die profile) is larger for HC than for LC. This difference in thickness strain distribution between HC and LC can be qualitatively explained from the difference in the shapes of the work contours, as shown in Fig. 3. The difference in flow stresses between the top (equibiaxial tension) and the periphery (plane strain tension) is smaller for HC than for LC; therefore, the plane strain elongation at the periphery is accelerated more for HC than for LC. Accordingly, the thickness reduction at the periphery becomes larger for HC than for LC. Thus, the difference in crystallographic texture causes the relative difference in the magnitude of flow stress between the equibiaxial tension and plane strain tension and, consequently, causes the difference in

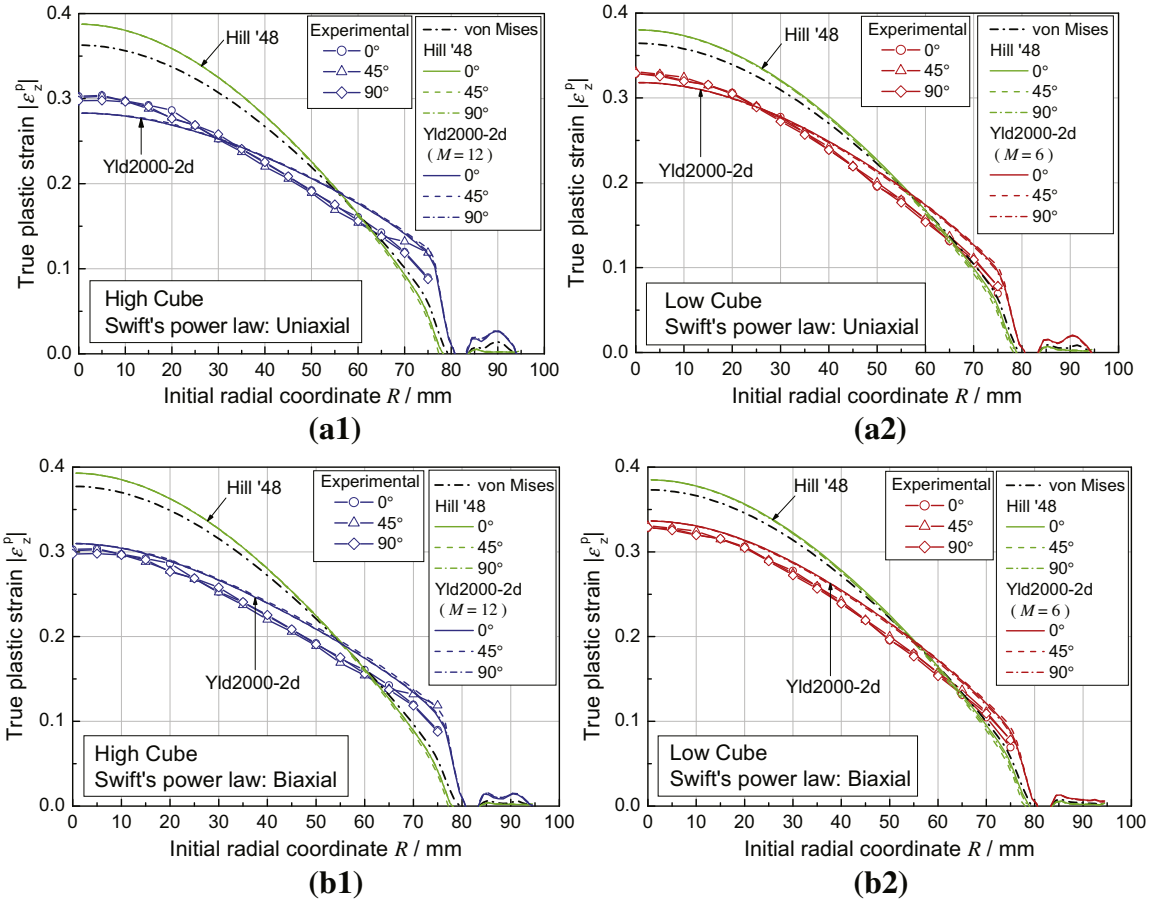

Fig. 9. Measured thickness strain along the meridian lines of bulged specimens compared with those calculated using FEA with selected yield functions.

the thickness distribution along the radial direction of the bulged specimen for the two materials.

Comparison of the reduction in the experimental and calculated thickness indicates that the Yld2000-2d yield function is capable of reproducing the experimental tendency with good accuracy for both materials, and has closer agreement with the experimental results than other yield functions, regardless of the work hardening laws used in the FEA. In contrast, both the von Mises and Hill's quadratic yield functions overestimate and underestimate the thickness reduction at the top and periphery, respectively, which results in a large deviation from the experimental results. The difference in thickness between the top and periphery is in the order of Hill '48 > Von Mises > Yld2000-2d. This is in accordance with the order for the difference of flow stress between equibiaxial tension (at the top) and plane strain tension (at the periphery) with each yield function. The results in Fig. 9 correspond with those in Fig. 3. Thus, it is concluded that the biaxial tensile testing method with cruciform specimens is effective for characterization of the deformation behavior of sheet metals in the first quadrant of the principal stress space. In this study, the appropriate yield functions were determined using the biaxial tensile testing method. We successfully improved the predictive accuracy of the FEA simulations using the determined yield functions for the stretch-forming of the test materials.

Comparing the FEA results in Fig. 9(a) and (b) shows that the results calculated using the Yld2000-2d yield functions shown in Fig. 9(b1) and (b2) are in closer agreement with the measurement than those in Fig. 9(a1) and (a2). Thus, the work hardening equation to be used for the FEA should be determined from the biaxial stress test that closely reproduces the stress states that occur in actual sheet forming operations.

Isotropic hardening was assumed in the FEA; however, as shown in Fig. 3, the assumption of isotropic hardening does not correctly reproduce the work hardening behavior of the test materials. As one method to numerically reproduce the differential work hardening behavior shown in Fig. 3, a model can be used in which the parameters of the Yld2000-2d yield function change as a function of ε_0^p or the plastic work, W_0. However, the biaxial tensile testing method using a cruciform specimen is not useful for that purpose, because the maximum plastic strain applied to the cruciform specimen is several percent at most, which is far below that applied to the bulged specimen. Ishiki et al. (2008, 2011) and Enatsu and Kuwabara (2011) proposed an alternative biaxial testing method that is capable of applying much larger plastic strain to a sheet specimen. A tubular specimen is fabricated by bending an original sheet sample and welding the bent sheet edges to each other, and an axial force and internal pressure are applied to the tubular specimen using a servo-controlled tube bulge testing machine. Thus, biaxial stress-strain curves under an arbitrary stress ratio, up to much larger strain range than those attained using a cruciform specimen, can be measured. More accurate FEA simulations could be obtained using such a material model that is capable of accurately reproducing the work hardening behavior up to a higher strain range. We have begun preliminary tube bulge tests using aluminum alloy sheet and have been successful in measuring biaxial stress-strain curves up to over 10% strain (Yanaga et al., 2012), of which the experimental and material modeling results will be published in the near future.

7. Conclusions

(1) Biaxial tensile tests of 6000 series aluminum alloy sheets with different density cube textures (HC and LC) were conducted using cruciform specimens. The difference in crystallographic texture was clearly detected as the difference in the plastic deformation behavior from biaxial tensile tests; the shapes of the work contours and the directions of the plastic strain rates were in good agreement with those calculated using the Yld2000-2d yield function. The appropriate value of the exponent M, for the Yld2000-2d yield functions changed with increasing ε_0^p; the value of M increased from 6 (ε_0^p =0.002) to 12 (ε_0^p =0.040) for HC, and from 4 (ε_0^p =0.002) to 6 (ε_0^p =0.045) for LC.

(2) The thickness strain distribution along the meridian lines on the bulged specimens were measured and compared with those calculated using FEA. The FEA results based on the Yld2000-2d yield function, which had better reproducibility of the biaxial tensile test results than other yield functions, are in closer agreement with the measured thickness strain distribution for both materials.

(3) It is thus concluded that the biaxial tensile testing method using a cruciform specimen is an effective material testing method to accurately detect and model the deformation behavior of sheet metals under biaxial tension. Therefore, the determination of an appropriate yield function based on the biaxial tensile test is useful to improve the predictive accuracy of FEA for aluminum alloy sheet forming processes.

(4) For the improvement of the accuracy of FEA, the work hardening equation used for the FEA should be determined from the biaxial stress test that closely reproduces the stress state occurring in the actual sheet forming operation.

Acknowledgment

The authors are grateful to Professor Jeong Whan Yoon of the Swinburne University of Technology for kindly providing the subroutine program for the Yld2000-2d yield function used in the FEA.

References

Abaqus Analysis, 2009. User's Manual, Version 6.9, Dassault Systems.

Banabic, D., Barlat, F., Cazacu, O., Kuwabara, T., 2010. Advances in anisotropy and formability. Int. J. Mater. Form. 3, 165–189.

Barlat, F., 1987. Crystallographic texture, anisotropic yield surfaces and forming limits of sheet metals. Mater. Sci. Engng. 91, 55–72.

Barlat, F., Brem, J.C., Yoon, J.W., Chung, K., Dick, R.E., Lege, D.J., Pourboghrat, F., Choi, S.H., Chu, E., 2003. Plane stress yield function for aluminum alloy sheets – Part 1: Theory. Int. J. Plasticity 19, 1297–1319.

Barlat, F., Aretz, H., Yoon, J.W., Karabin, M.E., Brem, J.C., Dick, R.E., 2005. Linear transformation-based anisotropic yield functions. Int. J. Plasticity 21, 1009–1039.

Enatsu, R., Kuwabara, T., 2011. Biaxial tensile test of cold rolled if steel sheet for large plastic strain range. In: Proceedings of the 8th International conference and workshop on Numerical Simulation of 3D Sheet Metal Forming Processes (AIP Conference Proceedings, vol. 1383), Seoul, Korea, pp. 565–570.

Hanabusa, Y., Takizawa, H., Kuwabara, T., 2010. Evaluation of accuracy of stress measurements determined in biaxial stress tests with cruciform specimen using numerical method. Steel Res. Int. 81, 1376–1379.

Hanabusa, Y., Takizawa, H., Kuwabara, T., 2011. Numerical verification in biaxial stress tests using cruciform specimen. J. Jap Soc. Tech. Plasticity 52, 282–287 (in Japanese).

Hashimoto, K., Kuwabara, T., Iizuka, E., Yoon, J.-W., 2010. Effect of anisotropic yield functions on the accuracy of hole expansion simulations for 590 MPa grade steel sheet. Tetsu-to-Hagané 96, 557–563 (in Japanese).

Hill, R., 1948. A theory of the yielding and plastic flow of anisotropic metals. Proc. Royal Soc. London A193, 281–297.

Hill, R., Hutchinson, J.W., 1992. Differential hardening in sheet metal under biaxial loading: a theoretical framework. J. Appl. Mech. 59, S1–S9.

Hill, R., Hecker, S.S., Stout, M.G., 1994. An investigation of plastic flow and differential work hardening in orthotropic brass tubes under fluid pressure and axial load. Int. J. Solids Struct. 31, 2999–3021.

Ishiki, M., Kuwabara, T., Yamaguchi, M., Maeda, Y., Hayashida, Y., 2008. Differential work hardening behavior of pure titanium sheet under biaxial loading. In: Hora, P. (Ed.), Proceedings of the 7th International conference and workshop on Numerical Simulation of 3D Sheet Metal Forming Processes. Institute of Virtual Manufacturing, ETH Zurich, Switzerland, pp. 161–166.

Ishiki, M., Kuwabara, T., Hayashida, Y., 2011. Measurement and analysis of differential work hardening behavior of pure titanium sheet using spline function. Int. J. Mater. Forming 4, 193–204.

Kuwabara, T., Ikeda, S., Kuroda, T., 1998. Measurement and analysis of differential work hardening in cold-rolled steel sheet under biaxial tension. J. Mater. Process Technol. 80–81, 517–523.

Kuwabara, T., Kuroda, M., Tvergaard, V., Nomura, K., 2000. Use of abrupt strain path change for determining subsequent yield surface. Experimental study with metal sheets. Acta Mater. 48, 2071–2079.

Kuwabara, T., Van Bael, A., Iizuka, E., 2002. Measurement and analysis of yield locus and work hardening characteristics of steel sheets with different r-values. Acta Mater. 50, 3717–3729.

Kuwabara, T., 2007. Advances in experiments on metal sheets and tubes in support of constitutive modeling and forming simulations. Int. J. Plasticity 23, 385–419.

Kuwabara, T., Hashimoto, K., Iizuka, E., Yoon, J.-W., 2011. Effect of anisotropic yield functions on the accuracy of hole expansion simulations. J. Mater. Processing Technol. 211, 475–481.

Moriya, T., Kuwabara, T., Kimura, S., Takahashi, S., 2010. Effect of anisotropic yield function on the predictive accuracy of surface deflection of automotive outer panels. Steel Res. Int. 81, 1384–1387.

Von Mises, R., 1913. Mechanik der festen Korper un plastich deformablen Zustant. Göttingen Nachrichten, math.-phys. Klasse, 582–592.

Yanaga, D., Kuwabara, T., Uema, N., Asano, M., 2012. Biaxial work hardening characteristics of 6000 series aluminum alloy sheet for Large Strain Range. Proc. MSEC 2012. (accepted).

Yoon, J.W., Barlat, F., Dick, R.E., Chung, K., Kang, T.J., 2004. Plane stress yield function for aluminum alloy sheets—part II: FE formulation and its implementation. Int. J. Plasticity 20, 495–522.

Yoon, J.W., Barlat, F., Dick, R.E., Karabin, M.E., 2006. Prediction of six or eight ears in a drawn cup based on a new anisotropic yield function. Int. J. Plasticity 22, 174–193.

Yoshida, K., Ishizaka, T., Kuroda, M., Ikawa, S., 2007. The effects of texture on formability of aluminum alloy sheets. Acta Mater. 55, 4499–4506.